Journal of Power Sources 245 (2014) 501–509

Contents lists available at SciVerse ScienceDirect

Journal of Power Sources

journal homepage: www.elsevier.com/locate/jpowsour

Faceted *shape-drive* cathode particles using mixed hydroxy-carbonate precursor for mesocarbon microbeads *versus* $LiNi_{1/3}Mn_{1/3}Co_{1/3}O_2$ Li-ion pouch cell

P. Manikandan, P. Periasamy, R. Jagannathan*

Lithium Batteries – Electrochemical Power Sources Division, CSIR-Central Electrochemical Research Institute, Karaikudi 630 006, TN, India

HIGHLIGHTS

- W-weaving Li-ion pouch cell designed, demonstrated under loads 0.12 Wh, 1.1 Wh.
- Facile route for activity enhanced cathode particles for Li-ion pouch cell.
- Activity enhanced, faceted cathode-particles explained through *shape-drive*.
- Li *vs* $LiNi_{1/3}Mn_{1/3}Co_{1/3}O_2$ cell delivered discharge capacity of 187 mAh g^{-1}.
- High hexagonal ordering, low cation mixing through $I_{(003)}/I_{(104)} = 1.8$.

GRAPHICAL ABSTRACT

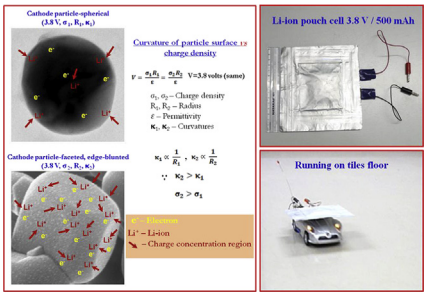

ARTICLE INFO

Article history:
Received 21 May 2013
Received in revised form
21 June 2013
Accepted 21 June 2013
Available online 2 July 2013

Keywords:
Mixed hydroxy-carbonate
Layered cathode material
Charge density
Li-ion pouch cell

ABSTRACT

Using a mixed hydroxy-carbonate (MHC) precursor, homogeneous $LiNi_{1/3}Mn_{1/3}Co_{1/3}O_2$ phase synthesized through a facile route yielded well dispersed, faceted, edge-blunted polyhedral particles (~200 nm). These cathode particles revealed high degree of hexagonal ordering favorable for impressive electrochemical performance *viz.*, high capacity 187 mAh g^{-1} in Li *vs* $LiNi_{1/3}Mn_{1/3}Co_{1/3}O_2$ cell, not fortuitously. Rather, can be clearly attributed to edge-blunted cathode particles that may facilitate enhanced charge mobility mimicking a process akin to corona discharge predominantly in charge concentrated regions which contrasts to moderate capacity from spherical particles explainable under the ambit of *shape-drive* hither to unknown. Li-ion pouch cell (~500 mAh) fabricated with this activity enhanced cathode quite rugged enough to endure loads (0.12 Wh, 1.1 Wh), as-demonstrated.

1. Introduction

Since the advent of Li-ion batteries in portable electronic devices in the early 1990s [1], Li-ion battery community have been endeavoring to address several challenges *viz.*, toxicity, cost, high capacity, health and safety issues [2,3] to achieve more affordable eco-friendly electrochemical power system(s). Most of these challenges are met through sustained research and development on Li-ion battery components, in particular the choice on cathode systems eventually paving way for new potential cathode systems such as *olivine* $LiFePO_4$, *spinel* $LiMn_2O_4$, *layered* $LiNi_{1/3}Mn_{1/3}Co_{1/3}O_2$ with the genesis of cathode materials tracing from the toxic $LiCoO_2$. Of these, electrochemical performance of $LiNi_{1/3}Mn_{1/3}Co_{1/3}O_2$ (for reasons of brevity labeled as LNMC henceforth) cathode system

* Corresponding author. Tel.: +91 4565241507, +91 9487167780; fax: +91 4565227713.
E-mail addresses: periasamylibatt@gmail.com (P. Periasamy), jaganr_57@yahoo.co.in, jags57_99@yahoo.com (R. Jagannathan).

0378-7753/$ – see front matter © 2013 Elsevier B.V. All rights reserved.
http://dx.doi.org/10.1016/j.jpowsour.2013.06.126

stands apart in terms of high cell voltage, capacity coupled with impressive structural stability and excellent cycling performance [4,5]. These distinguishing features make this cathode system very attractive for eventual application in batteries. There are numerous trials reporting syntheses of LNMC such as solid state [6], sol–gel [7], combustion [8], molten salt method [9], micro emulsion [10], rheological phase [11] methods yielding cathode particles having different morphologies.

Notwithstanding extensive work on LNMC system, there are several attended problems *viz*., toxic gases generated during the course of the synthesis, lack of control on particle size, dispersibility of the materials. These short comings do limit the application scope of the LNMC system. Bearing these important issues in mind we are motivated to try a more eco-friendly synthesis strategy for developing LNMC cathode system. In most of the known methods, toxic gases generated during the course of calcination rests with the precursor employed. However solid state method stands unique in not generating any toxic gases but with the drawback of lower electrochemical performance attributed to not so homogeneous chemical composition, coarser particles. We thought these drawbacks can be overcome when the solid state reaction is preceded by a homogeneous wet-chemical co-precipitation reaction ensuring atomic scale-mixing of Ni, Mn and Co ion constituents apart from non toxic gaseous by-products *viz*., water, carbon dioxide. Also it turns out that the co-precipitate comprising mixed hydroxy-carbonates of LNMC transition metals can lead to oxidic cathode products having high dispersibility [12] owing to the evolution of non-toxic gases upon decomposition.

There is extensive literature reporting high capacity for Li-ion batteries ascribed to factors like synthesis methods, parameters [13,14] precursors employed [15,16] and so on. We consider the particle morphology in particular presence of sharp-edges present in the cathode particle has very crucial role in determining the efficiency of electrode–electrolyte charge transfer, in particular lithium (de)intercalation properties. Because this may constitute an important trait for evaluating electrochemical performance of Li-ion batteries, we devote an exclusive section focusing on particle shape under the ambit of *shape-drive* in cathode particles in comparison with related results available in the literature [15,16].

Another major daunting task concerning the design of Li-ion batteries is excessive weight of metallic cell casings which when stacked in large numbers limit the scope for large-scale application. However, the issue of excessive weight of the casings can be overcome through alternative design [17] based on pouches made of aluminum foil. Taking stock of this scenario in the design of Li-ion batteries, we present our results on Li-ion pouch cell fabricated with the LNMC cathode system.

2. Experimental aspects

In this work the cathode material has been synthesized through a facile route comprising two steps with (i) synthesis of precursor underlying co-precipitation of mixed hydroxy-carbonates of Ni, Mn and Co ions followed by (ii) optimized calcination of the precursor yielding the oxidic cathode products for being used in pouch cell application as schematized (Fig. 1): $(Ni_{1/3}Mn_{1/3}Co_{1/3})_2(OH)_2CO_3$ precursor was synthesized using stoichiometric aqueous solutions of $Ni(NO_3)_2\cdot 6H_2O$, $Mn(NO_3)_2\cdot 4H_2O$ and $Co(NO_3)_2\cdot 6H_2O$ (Merck AR grade). This mixed solution was slowly added to a mixture of NaOH (2 mol) and Na_2CO_3 (1 mol) aqueous solution at 40 °C under lab ambient conditions (air atmosphere) through stirring until complete precipitation appearing as green dark brownish gelatinous precipitate, which was filtered, washed using distilled water and ethanol followed by drying at 60 °C for 24 h resulting in the mixed hydroxy-carbonate (MHC) precursor. Then, stoichiometric amounts

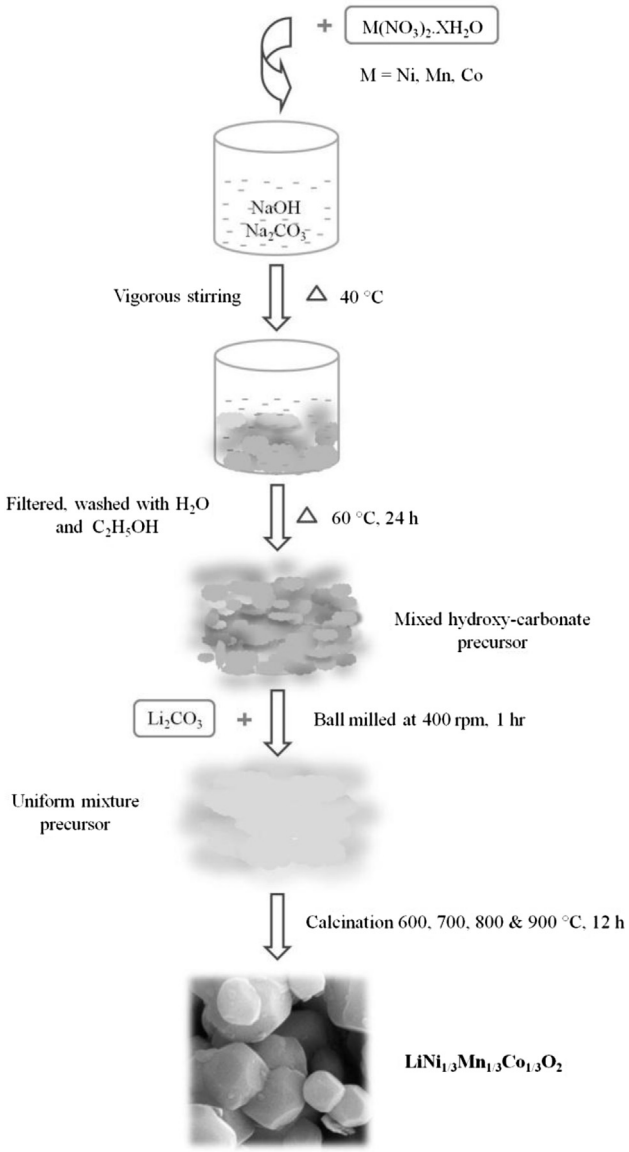

Fig. 1. Flow chart on the synthesis of LNMC cathode materials using MHC precursor.

of this MHC precursor and Li_2CO_3 were homogenized and ground well for 1 h using FRITSCH pulverisette 7 instrument at 400 rpm. After the homogenization step, this blend was calcined at a temperature 600, 700, 800 and 900 °C for 12 h to get LNMC cathode material for further investigation. Upon calcination, the thermal decomposition of the starting materials blend of MHC and Li_2CO_3 can be visualized through the following reaction.

$$Li_2CO_3 + \left(Ni_{1/3}Mn_{1/3}Co_{1/3}\right)_2(OH)_2CO_3 + \frac{1}{2}O_2 \xrightarrow{\Delta(600-900^\circ C)} 2LiNi_{1/3}Mn_{1/3}Co_{1/3}O_2 + 2CO_2\uparrow + H_2O\uparrow \quad (1)$$

Chemical purity of the as-prepared sample has been ascertained through powder X-ray diffraction studies using a Bruker D8 Advance X-ray diffractometer with a Cu Kα X-ray source ($\lambda = 1.5418$ Å) and the measurements were recorded with 2θ range 10–80°. Crystallite size of the cathode particles obtained after calcinations at different temperatures have been estimated using

XRD line broadening data in conjunction with Debye–Scherrer formula. During crystallite size estimate, correction for experimental broadening of the XRD line was done through subtraction of line width value of the corresponding bulk sample having an average particle size ~2 μ (with corundum Al_2O_3 as the internal standard). Various functional groups present in the precursor and also in the cathode material have been analyzed using FT-IR spectra measured on BRUKER Optik GmbH MODEL TENSOR 27 FT-IR spectrometer with a detector RT DLaTGS using a KBr pellet in the range 400–4000 cm^{-1}. Morphology of the precursor and cathode materials was analyzed through field emission scanning electron microscopy (FE-SEM) MODEL ZEISS SUPRA™ 55VP. Magnetic centers present in these samples were analyzed using electron paramagnetic resonance (EPR) with a Bruker EMX plus X-band EPR spectrometer.

Turning to electrochemical characterization, cyclic voltammograms (*CV*) were recorded using IVIUMnSTAT electrochemical workstation at a scan rate of 0.1 mV s^{-1} in the voltage range of 2.5 and 4.6 V under CR2032 cell configuration. Galvanostatic charge–discharge studies were made using Arbin multichannel cycler instrument (BT2000). Coin cells (half cell) were assembled using lithium foil (thickness: 0.75 mm) as anode and as-prepared LNMC material coated on Al foil as cathode. This was further extended to full cell configuration also.

More important, Li-ion pouch cell with Celgard® 2340 separator (W-weaving style) folding has been fabricated using six (four double-sided and two single-sided coated) negative electrodes and five (double-sided) positive electrodes inside a laminated pouch. In this trial, active materials of the negative and positive electrodes were mesocarbon microbeads (MCMB, MTI Corporation) and LNMC, respectively and 1 M solution of $LiPF_6$ in 1:1 (v/v) EC–DMC mixture was used as the electrolyte. In the fabrication of Li-ion pouch cell, important design parameters *viz*., electrode area (double side), electrode thickness (with current collector) and materials weight loading per side of the negative/positive electrodes were respectively 5 × 5 cm^2, 147/142 μ and 0.3285/0.4631 g (including carbon and binder) using LNMC cathode materials calcined at 900 °C. Furthermore the cathode was fabricated through doctor blade-coating slurry of 80% LNMC, 15% SP-carbon (Timcal) and 5% PVdF in NMP coated over aluminum foil (15 μ). The anode was fabricated using 95% MCMB with 5% PVdF binder in NMP slurry coated over copper foil (9 μ) and dried at 85 °C for 12 h in a vacuum oven. Both coin and pouch cells were assembled in an argon-filled glove box (mBRAUN MB200G) with oxygen and moisture levels less than 0.1 ppm. Cell performance of the coin cells were evaluated through charge–discharge studies in the range of 2.5 and 4.6 V at 0.1, 0.2, 0.5, 1 C and 2 C rates at room temperature. The performance of the fabricated pouch cell has been investigated through charge–discharge studies and also further used in demonstration kits *viz*., operation of LED array, electronic toy-car.

3. Results and discussion

In the synthesis of a given cathode material, chemical route employed holds the key in determining the electrochemical performance during application. That is, the cathode material synthesized through a conventional solid state reaction method entailing in coarser particles shows lower electrochemical performance [6] in comparison to finer particles synthesized through wet-chemical route(s) [10,15,16]. In a wet-chemical synthesis, co-precipitation under near neutral condition is more advantageous over basic conditions because the former results in more dispersible homogeneous particles of the target phase. Synthesis under basic conditions pH > 7 would accelerate the scope for hydroxide-gel formation that might hamper the dispersion of target particles especially in the absence of carbonaceous phases generating gaseous carbon dioxide during the course of the calcination. With this simple chemical condition in mind, the present work was based on mixed hydroxy-carbonate as the precursor for the synthesis of LNMC cathode. Furthermore this route has inherent advantages such as feasibility, batch-size up scalability (~50 g in lab-scale) and so on. This facile route requiring shorter milling time (~1 h) has an edge over conventional solid state route in terms of size tunability, homogeneous product without formation of secondary phases facilitating higher electrochemical capacity.

3.1. Structural parameters using XRD

An examination of Fig. 2 depicting identical X-ray powder diffraction patterns of samples prepared through calcinations at different temperatures as indicated, singular phase corresponding to LNMC cathode indexable under the space group $R\bar{3}m$ adopting α-$NaFeO_2$ type structure is obvious. Crystallographic unit cell parameter values deduced through least squares refinement of these XRD pattern(s) yielded cell parameter values *a*, *c*, consistent with the literature reports [18] as listed in Table 1. Also turning to growth of particles–crystallites, some insights become possible with estimate of crystallite size made through Debye–Scherrer XRD line broadening data, which yielded well dispersed large particles when calcined at 900 °C (Φ_{ave} = 143 nm). These apart, drastic changes observed in the relative line-intensity of these XRD patterns merit discussion: because this can yield wealth of information pertaining to rhombicity of the crystal structure in turn influencing lithium (de)intercalation processes, undesirable cation mixing hence electrochemical features in a significant way. In particular the relative intensity ratio of $I_{(003)}/I_{(104)}$ is very important with this ratio when being greater than 1.2 can yield favorable conditions such as least cation mixing owing to perfect hexagonal ordering coupled with pronounced lithium (de)intercalation processes [13]. On closer scrutiny XRD results of the present work we have that, the $I_{(003)}/I_{(104)}$ ratio is found to be 1.8021, being the highest for the sample calcined at 900 °C. This is quite favorable for good cathode performance as indeed is the case, it turned out to be. On the other hand the intensity ratio found to be much lower *viz*., 1.26, 1.39 for the sample prepared respectively through solid

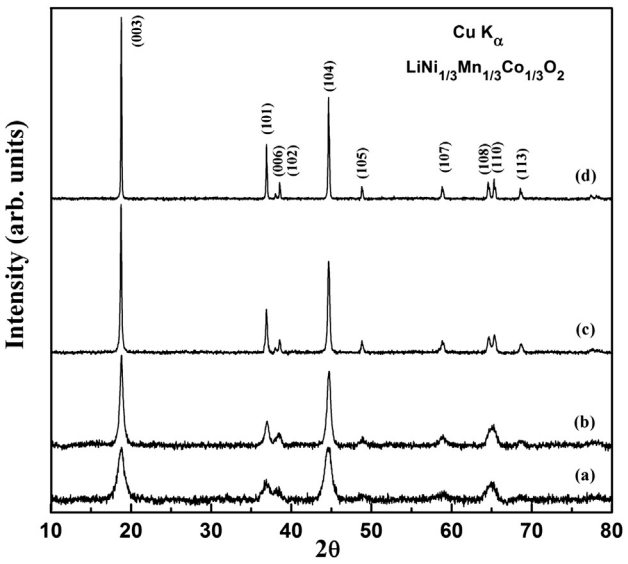

Fig. 2. Powder X-ray diffraction patterns of LNMC using MHC precursor calcined at (a) 600, (b) 700, (c) 800 and (d) 900 °C for 12 h.

Table 1
XRD structural parameters of LNMC materials calcined at 600–900 °C.

Calcined temperature	Crystallite size (nm)	a (Å)	c (Å)	c/a	V (Å)^3	$\frac{I_{003}}{I_{104}}$	$R = \frac{I_{006}+I_{102}}{I_{101}}$
600 °C	22	2.8616	14.1711	4.9521	100.49	0.9664	–
700 °C	51	2.8564	14.1537	4.9550	100.01	1.2556	–
800 °C	89	2.8562	14.1933	4.9692	100.27	1.6463	0.4016
900 °C	143	2.8597	14.1555	4.9499	100.25	1.8021	0.3019

state [6,19], sol–gel method [7] suggesting decreased scope for undesirable cation mixing. Furthermore, for the sample synthesized at 900 °C the doublet splitting observed in the XRD pattern corresponding to (006), (102) and (108), (110) pairs is a clear pointer to perfect hexagonal ordering coupled with good crystallinity. Also, the lower value observed for $R = (I_{006} + I_{102})/I_{101}$ of the sample calcined at 900 °C over sample calcined at 800 °C confirms again higher hexagonal ordering [20] for the former eventually paving way for better electrochemical performance.

3.2. Insights on functional groups

FT-IR spectral data on these inorganic compounds $(Ni_{1/3}Mn_{1/3}Co_{1/3})_2(OH)_2CO_3$ precursor and LNMC yield reliable information on various functional group present and their modes of interaction/vibration. As seen in Fig. 3a, the precursor material exhibits characteristic frequencies corresponding to stretching ν(O–H) at 3400 cm^{-1} over lapped with stretching vibration ν(O–H) of H_2O (Fig. 3a inset) mode of vibration indicating all hydroxy groups in the hydroxy-carbonates are hydrogen bonded (blue trace in Fig. 3a) in good agreement with literature reports [12]. The presence of δ(O–H) bending vibration of water vapor at 1634 cm^{-1} suggesting to trace amounts of absorption water in the electrode materials [21]. Also in this precursor material, carbonate group signatures revealed through 4 modes of vibrations *viz.*, $\nu_1(CO_3^{2-})$ symmetric stretching vibration) at 1060 cm^{-1}, $\nu_2(CO_3^{2-})$ out-of-plane deformation vibration) at 861 cm^{-1}, $\nu_3(CO_3^{2-})$ asymmetric stretching vibration) at 1420 cm^{-1} and $\nu_4(CO_3^{2-})$ in-plane deformation vibration) at 734 cm^{-1} are consistent with reports on carbonate group FT-IR data [12,22]. These data reliably confirm the formation of mixed hydroxy-carbonate in the thus synthesized precursor used for LNMC synthesis. Turning to the spectral data on cathode material (calcined at 900 °C indicated using red trace in Fig. 3a) hydroxy, carbonate groups are totally absent owing to the complete thermal decomposition of the precursor material. However we observe a clear proof for the occurrence of metal oxygen M–O bond vibrations assignable under different characteristic modes: asymmetric stretching $\nu(MO_6)$ at 597 cm^{-1} [23] and bending vibrations δ(O–M–O) at 543 cm^{-1} thereby confirming chemical integrity of the intended LNMC phase [24].

3.3. Paramagnetic center in LNMC cathodes

EPR spectroscopy is a reliable tool in probing the local electronic structure of paramagnetic species having unpaired spin components. It turns out that, of the various constituents of LNMC cathode Mn^{4+} ion having $3d^3$ electronic configuration generates intense paramagnetic signal. The electrochemical performance of the LNMC system having profound dependence on the synthesis procedure, in turn influenced by the cationic distribution in oxides [25]. Accordingly this technique provides useful information on Ni^{2+}, Mn^{4+} ion distribution and hence has been successfully used for the determination of the cationic distribution in the LNMC cathode system crystallizing under layered hexagonal compounds [26] with the Co^{3+} ions adopting a low-spin configuration ($S = 0$). The apparent g-factor is insensitive to the Co content with a value $g = 2.033$ for the LNMC system [27] with the LNMC system containing two magnetic ions, Ni^{2+} and Mn^{4+}. Ni^{2+} is a non-Kramer ion because it has even number of d-electrons and its EPR spectra is very sensitive to the interactions with the environment. Hence the EPR signal of Ni^{2+} can then be detected only when this ion is present as a residual impurity [28].

Using EPR as a powerful local probe (in both low and high frequency configurations) Shinova et al., have made extensive studies on the distribution of cationic sites in this important LNMC cathode system. In this report they have systematically demonstrated the effect of synthesis temperature in influencing EPR signals of different cations [29]. In the present work it turns out that when the concentration of these ions is large as in the present case, the distribution of crystal fields and strains on the different sites smear out the resonance spectra which are no longer detected. The

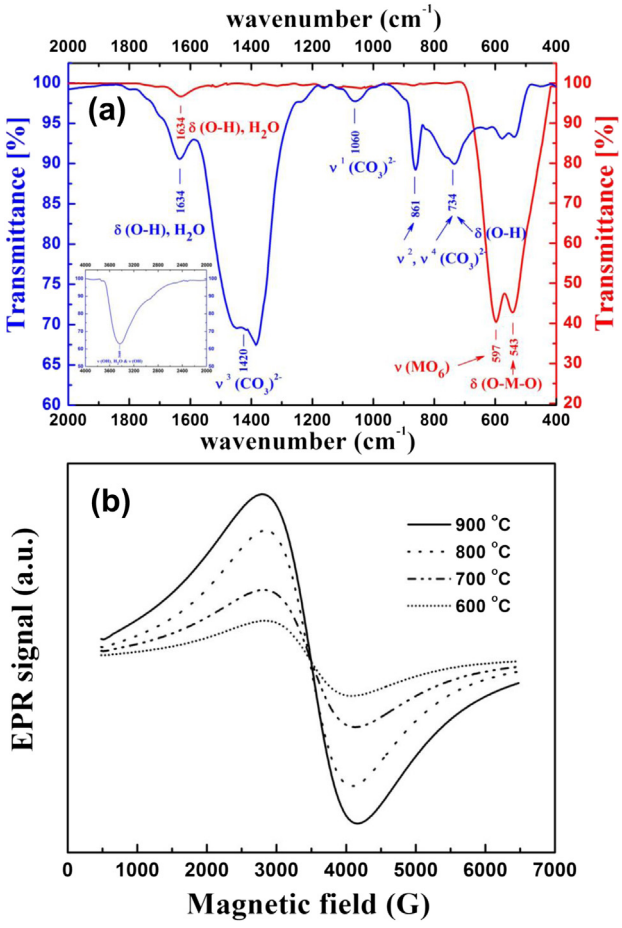

Fig. 3. (a) FT-IR spectra of MHC precursor (blue trace) [inset υ(OH) of MHC], LNMC materials calcined at 900 °C for 12 h (red trace) and (b) EPR spectrum of LNMC (600–900 °C for 12 h) at 25 °C and the position of the center of the signal is close to 3480 G as expected for uncorrelated spins with the gyromagnetic factor $g = 2.033$, for the microwave frequency (9.86 GHz). (For interpretation of the references to color in this figure legend, the reader is referred to the web version of this article.)

paramagnetic resonance detected can be attributed to the presence of Mn^{4+} ions which carry a half-integer spin ($S = 3/2$) and are then EPR-active. Increase in the synthesis temperature increases crystallinity eventually increasing both microscopic, macroscopic orderings of the lattice under investigation. Obviously, this would explain higher EPR signal strength for the sample synthesized at 900 °C than does for the sample synthesized at lower temperature *viz*., 600 °C as can be seen from the EPR spectra of the LNMC prepared through the facile route (Fig. 3b). The EPR spectrum of the pristine sample consists of only one signal with a Lorentzian line shape and is indicative of the ordered nature of the sample [30]. The position of the center of the signal is close to 3480 G. Also, the contributions from Ni^{3+} centers are expected to be absent in the LNMC system because Ni^{3+} is in the low-spin state [26] in particular when there is no smearing of EPR signal.

3.4. Dispersed, faceted, edge-blunted shape-drive cathode particles

With the quest for realizing theoretical capacity of 277 mAh g^{-1} eventually paving way for wide scope of applications demanding higher power, energy densities, lithium battery community has been endeavoring different strategies *viz*., miniaturization of particle size, tuning particle morphology, increasing hexagonal ordering, disorder induced through undesirable cation mixing and adopting different synthesis methodologies in/for the cathode system. It turns out that, the cathode particle having spherical morphology with size scaled down to 250 nm yielded a capacity of 171 mAh g^{-1} @ 0.08 C [31], also cathode particles having sharp edges stemming from brick type particle morphology having active facets [16] yielded high capacity of 180 mAh g^{-1} @ 1 C. It should also noted that for LNMC samples with minimized cation mixing (Li/Ni ordering), enhanced hexagonal ordering reflected through doublet splitting of (006), (102) and (108), (110) pairs of XRD lines yielded a high capacity of 187 mAh g^{-1} @ 20 mA [13]. Switching to more homogeneous wet chemical synthesis strategies such as micro emulsion [10], co-precipitation methods [15,16] also yielded the same high capacity. Different methodologies employed for the synthesis of this cathode system led to LNMC cathode system made of spherical particles which invariably showed lower capacity [31,32] when compared with higher capacity yielding sharp edged particles [10,16].

Turning to explain the uniqueness of results of our synthesis based on the MHC precursor: the product comprised highly dispersed LNMC cathode particles having regular faceted polyhedral morphology with size in the range of 200 nm (Fig. 4). We consider that the MHC precursor in spongy form (Fig. 4a) may facilitate homogeneous distribution along with Li_2CO_3 fine powders. Also, the generation of H_2O vapors, CO_2 gases upon decomposition of the precursor permeating throughout the volume of the reactants can lead to achieving well dispersed LMNC particles as the calcinations product (Fig. 4b). On a glance of the LNMC product (Fig. 4c–d), the highly dispersed particles having polyhedral morphology with sides of this particulate polyhedra regularly faceted with blunted/truncated edges obvious which has been highlighted using yellow traces (Fig. 4c–d).

3.5. Cyclic voltammetric investigations

Fig. 5a depicts the cyclic voltammetry profile of Li/LNMC cell in the voltage range 2.5–4.6 V @ 0.1 mV s^{-1}. It is obvious that the main oxidation peak can be located at 3.97 V, while the reduction peak can be traced at 3.53 V, corresponding to the Ni^{2+}/Ni^{4+} redox process. Furthermore, the occurrence of unique redox band observed at 3.97 V/3.53 V (as indicated in Fig. 5a) in the voltage range studied implies that there is no structural transition, especially from hexagonal to monoclinic phase, which is expected to limit the reversibility, charge/discharge capacity of the cathode system [13]. It is significant to note that there is no redox peak around 3 V region implying the absence of Mn ions in the 3+ state [19]. Turning to the interpretation of the *CV* traces of this study: the

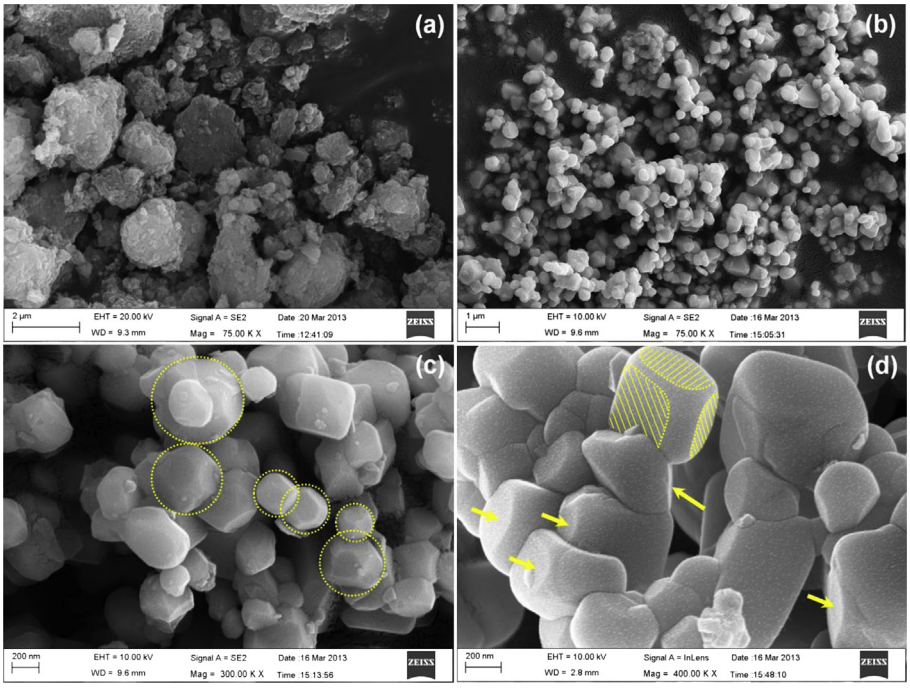

Fig. 4. FE-SEM image of (a) MHC precursor and (b–d) dispersed LNMC cathode materials calcined at 900 °C for 12 h. Images were recorded at 75, 300 and 400 K × magnifications respectively. Faceted, edge-blunted regions of cathode particles indicated using yellow traces (circles, lines and arrows). (For interpretation of the references to color in this figure legend, the reader is referred to the web version of this article.)

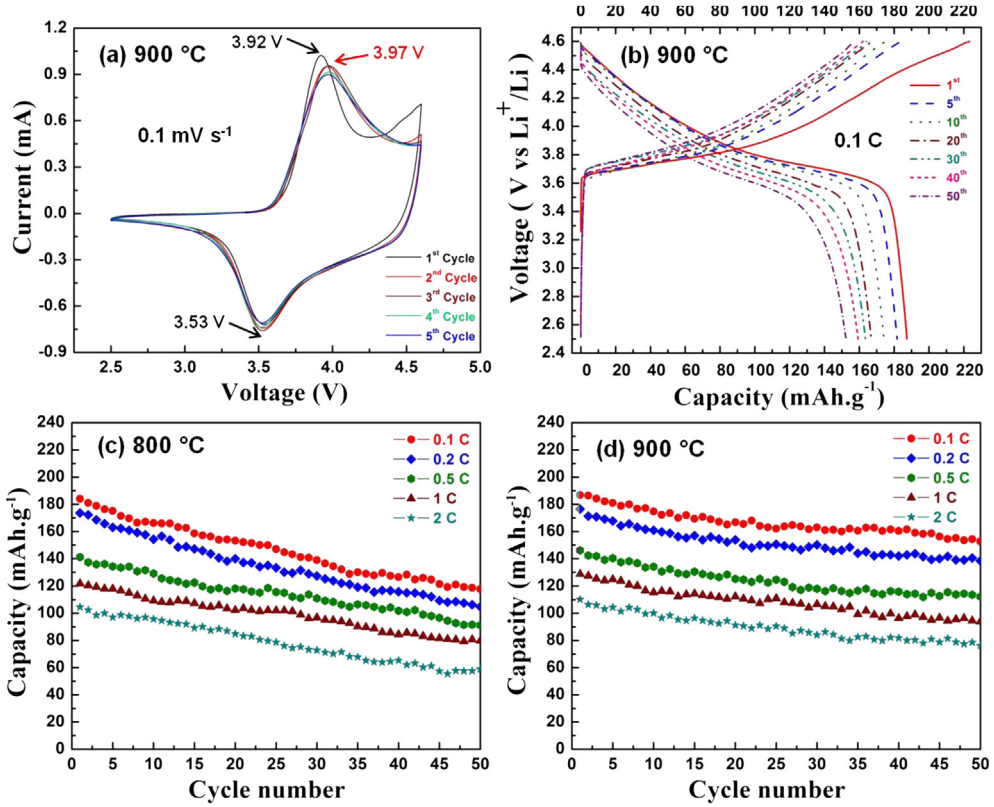

Fig. 5. (a) Cyclic voltammograms (0.1 mV s^{-1}), (b) voltage *vs* capacity profile for Li *vs* LNMC cells in the voltage range from 2.5 to 4.6 V at 0.1 C (1 M $LiPF_6$ in 1:1 EC–DMC solvents), (c) LNMC − 800 °C and (d) LNMC − 900 °C capacity *vs* cycle number performance at different rates: 0.1 C, 0.2 C, 0.5 C, 1 C and 2 C.

difference $\Delta\varphi_p$ between anodic peak potential φ_{pa} and cathodic peak potential φ_{pc} can be the measure of the reversibility of the intercalation process with low value of $\Delta\varphi_p = 0.39$ V enhancing the reversibility of redox process. In the initial scan the major anodic peak occurs at 3.92 V followed by shifting to 3.97 V and maintaining at this value in the subsequent scans. On the other hand, corresponding cathodic peak maintains at 3.53 V in all the studied cycles. The shift observed in the anodic peak can be rationalized by considering active electrolyte decomposition, passive film formation processes during first anodic scan. Summing up of results of the present *CV* studies, barring the initial cycle there is perfect overlap of *CV* traces in 2nd–5th scans indicating excellent reversibility for (de)intercalation of Li species [13]. Also the absence of obvious extra redox peak ensures chemical phase singularity of the synthesized cathode in corroboration with XRD studies. As good reversibility is the clear indicator of structural stability, the present *CV* results points to impressive robustness of the cathode synthesized through the facile route.

3.6. Charge–discharge studies

Charge–discharge study constitutes the most important step in evaluating the performance of any electrochemical system fabricated and feasibility for useful application. Accordingly, results of charge–discharge studies made for the electrochemical cell using the as-prepared LNMC cathode under 0.1 C rate, 2.5–4.6 V range upto 50 cycles are presented in Fig. 5b. This typical charge–discharge profile presents only one plateau in the voltage region ~4 V. This is consistent with the results of *CV* experiments as discussed in the previous section. The galvanostatic cycling behaviors of cathodes made with LNMC materials calcined at 800 °C and 900 °C for 12 h are depicted in Fig. 5c–d. From this cycling performance study, it is observed that LNMC electrode (synthesized at 900 °C) delivers higher discharge capacity for different C-rates such as 0.1 C, 0.2 C, 0.5 C, 1 C and 2 C along with smaller capacity fade than for the sample calcined at 800 °C. These results indicate that the sample calcined at 900 °C exhibits superior hexagonal ordering in conformity with structural parameters deduced using XRD (Table 1). More important, the present LNMC electrode delivered an initial discharge capacity of 187 mAh g^{-1} with an irreversible capacity loss of 36 mA during the 1st cycle. The charge–discharge capacities at 50th cycle are 154 and 153 mAh g^{-1} respectively. The capacity decay upon cycling is small (~1.2 mAh g^{-1} per cycle during the first five cycles), which progressively decreased with cycling (~0.3 mA per cycle at 46th–50th cycles). Significantly, the coulombic efficiency rises from 84% at 1st cycle to 99% at the 50th cycle. The capacity retention at the 50th cycle is about 82%. The capacity fading in this system of material can be correlated with progressively increasing surface passivation on LNMC electrode entailing in ohmic drop upon prolonged cycling. Turning to explain the mechanism of capacity fading, it is possible that the important cause may be dissolution of LNMC active material in the electrolyte during cycling which can be attributed to the generation of HF easily formed when using $LiPF_6$ as the electrolyte salt [33,34]. The discharge results are similar to the reported capacity decay of such materials subjected to high-temperature processing [35]. Thus observed superior performance can be attributed to the lower degree of undesirable cation mixing because coulombic efficiencies and charge–discharge performance which are related to cation mixing in the host structure. The decrease in capacity at higher C-rate (176 mAh g^{-1} @ 0.2 C, 147 mAh g^{-1} @ 0.5 C, 129 mAh g^{-1} @ 1 C and 110 mAh g^{-1} @ 2 C) can be rationalized in terms of limitations stemming from the dismal electronic and ionic conductivities of this LNMC system impeding free flow of charges.

3.7. Curvature sensitive shape-drive on charges in cathode particles

Accordingly, thus synthesized cathode particles when used a cathode in a Li-ion cell yielded impressive electrochemical performance: 187 mAh g^{-1} @ 28 mA. It does not seem fortuitous that better results realized in this work can be attributed to cathode materials synthesized through the new MHC as an alternative precursor. In this scenario it seems, reasonable to propose that cathode particles having sharp edges (both regular and irregular shapes like brick with facets, faceted polyhedra) always yielded higher capacity [16] that is higher rate of charge flow than particles having smooth surface (like spherical morphology) [31,32]. In other words, cathode particles having faces with blunted edges are more electrochemically active than smooth surfaces of spherical particles with the former exhibiting increased propensity for flow of charges. That is sharp edges and curved surfaces induce a great deal of activity enhancement than does a smooth surface. Also taking a cue classical theory on liquid drop formation it is important to note that for the given circumference or dimension of the particle(s), sphere has the lowest surface area without any sharp edges. Furthermore, comparison of surface areas between spherical (without any edges) and faceted (cuboidal with 12 edges) particles of same dimension (~200 nm) suggests a clear two fold increase for the latter. This could eventually enhance the propensity for the intense electrochemical/charge transfer processes.

In order to further explain the forgoing results precisely, it is worthwhile to invoke the basic concept of electrostatics underlying the relation between charge density *vs* curvature at a given potential [36,37]. We have that for an electrode surface at a given potential, charge density (σ) and curvature (κ) bear direct relation, in other words for surfaces having large radius of curvature the surface charge density is expected to be low and *vice versa*. For both spherical and faceted cuboidal particles of the given cathode material the potential (V) and also the permittivity (ε) are expected to be constants while the charge density (σ_1, σ_2) varies inversely with radius of curvature (R_1, R_2) rather directly with curvature (κ_1, κ_2). Obviously, faceted particles do have steep curvatures than does a spherical particle with the former showing enhanced tendency to acquire charges ($\kappa_2 > \kappa_1$, $\because \sigma_2 > \sigma_1$). This is indeed the case observed: faceted, edge-blunted cathode particles of the present study do show a convincing (~15%) enhancement in capacity (hence increases in flow/mobility of charges through a process akin to corona discharge) over spherical particles having larger radius of curvature [31,32] as has been schematized (Fig. 6). Summing up the forgoing results, shape of cathode particles holds the key in determining the cell performance in particular enhancing mobility of charge carriers for which reason we prefer to nomenclature the

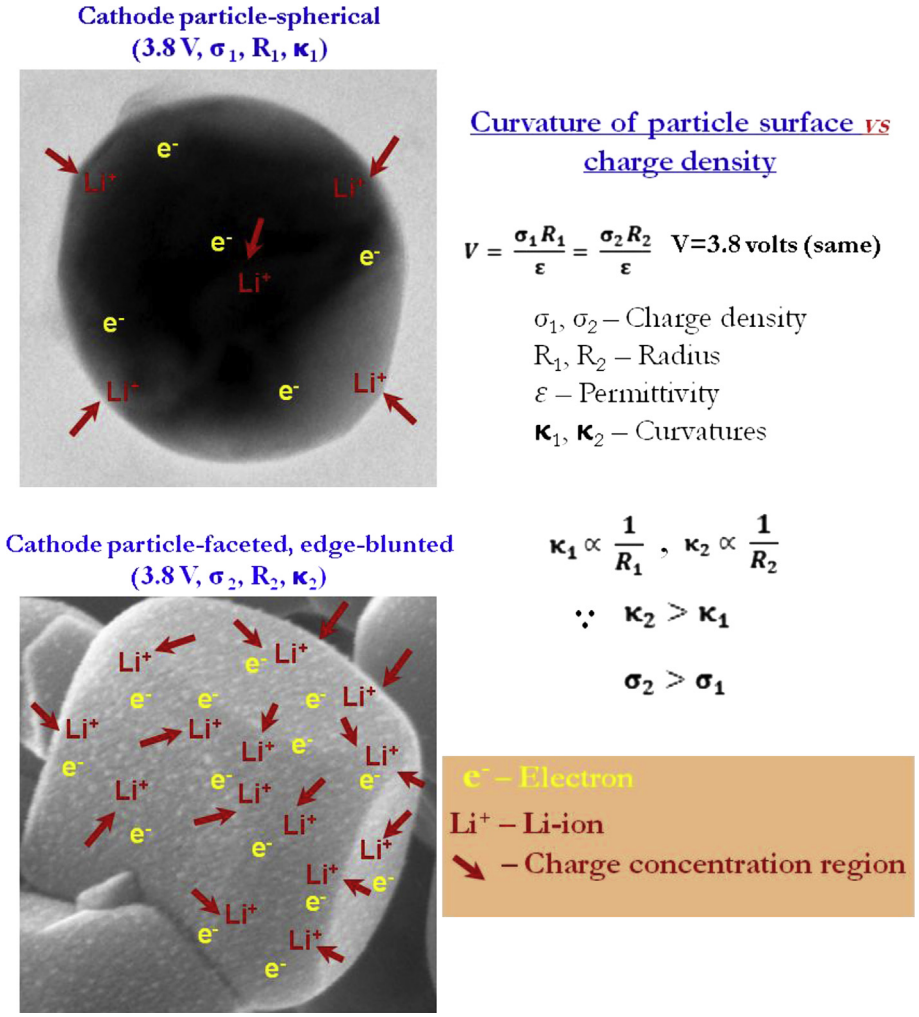

Fig. 6. Schematics illustrating the difference in electrochemical activity/charge flow between smooth surfaced (spherical) and sharp edged (faceted, edge-blunted) cathode particles.

shape driven/induced flow of charges as *shape-drive* in these activity enhanced particles.

3.8. Li-ion pouch cell: features and performance

Because Li-ion pouch cell has several advantages *viz.*, light weight, low cost, higher energy density meriting applications in stacking mode for electric vehicle applications [38] over other type of Li-ion cells the former has tremendous application potential. Electrochemical studies on the Li-ion pouch cell (MCMB/PP–PE–PP/LNMC) made in our lab exhibited a high cell capacity of ~500 mAh. After an aging of 24 h, this cell was used for further electrochemical studies. Turning to the electrochemical performance of Li-ion pouch cell, it is essential to pass through the formation cycle process at a low current rate of 0.02 C (@ 19 mA) for the first cycle comprising charging in two continuous steps *viz.*, constant current (CC), constant voltage (CV) modes [39]. The formation cycle (@ ~0.02 C, 19 mA) and cycling performance (@ ~0.1 C, 96 mA) of Li-ion pouch cell is shown in Fig. 7 (voltage *vs* time, current *vs* time). The former is charging up to 4.6 V at a given current while the latter following at 4.6 V with drawn current allowing only 5% rated capacity of the cell. The formation cycle is essential for stabilization of the active materials through solid electrolyte interface (SEI) film formation in the cell [39,40]. SEI film has the intrinsic advantage of preventing further chemical reaction between electrolyte and active materials. The life and discharge performance of the Li-ion pouch cell are highly dependent on the SEI formed over the carbon electrode during the formation process. It is expected that the applied low current (19 mA) can produce a denser SEI layer which is advantageous for improving cyclability of the Li-ion pouch cell. Extending our investigations to evaluate cell capacity performance, results pertaining to charge–discharge studies on the Li-ion pouch cell in the voltage range 2.5–4.6 V up to 50 cycles (@ ~0.1 C, 96 mA) are given in Fig. 8. Also it is important to monitor the performance of voltage *vs* cell capacity of this electrochemical power system having immense application potential and hence the same is given in the inset of Fig. 8. More important this pouch cell system shows remarkable maintenance in electrochemical cell capacity ~500 mAh even at 50th cycle. Elaborating further, this pouch cell delivered the discharge capacity of 525 mAh at 25th cycle in the voltage range 2.5–4.6 V (@ ~0.1 C, 96 mA). The capacity fade is similar to Li *vs* LNMC cells which can be explained in the same lines as discussed earlier. Owing to the

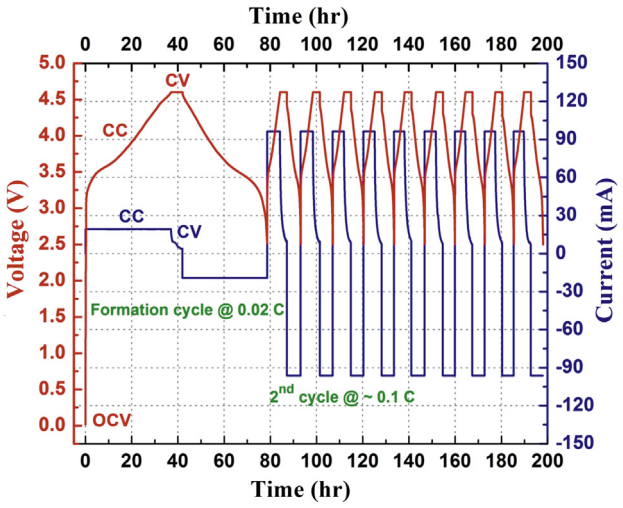

Fig. 7. Cycling performance of Li-ion pouch cell 3.8 V/500 mAh (voltage *vs* time, current *vs* time) in the voltage range from 2.5 to 4.6 V.

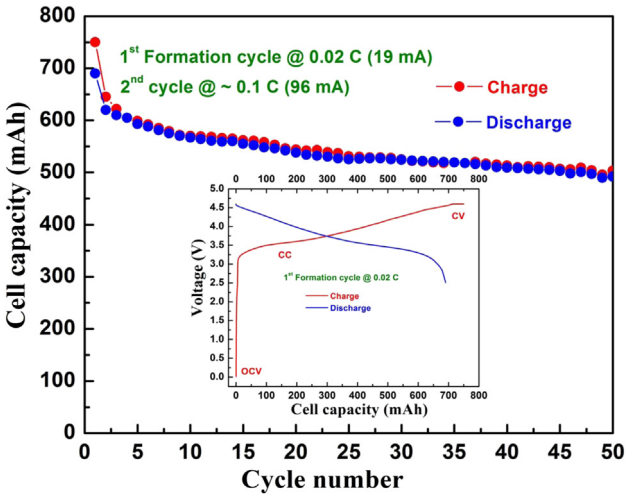

Fig. 8. Cell capacity *vs* cycle number performance of MCMB *vs* LNMC Li-ion pouch cell (3.8 V/500 mAh) in the voltage range 2.5–4.6 V up to 50 cycles (inset voltage *vs* cell capacity for formation cycle @ 0.02 C).

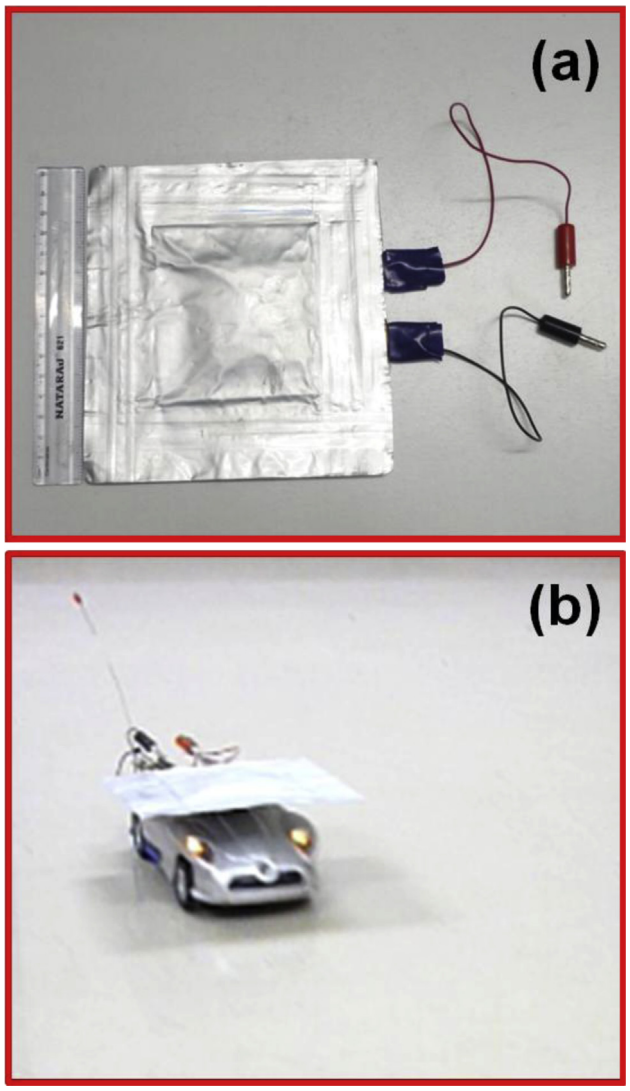

Fig. 9. (a) Demonstration of fabricated Li-ion pouch cell 3.8 V/500 mAh (b) the same pouch cell used to activate electronic toy-car running on tiled floor at CSIR-CECRI, INDIA.

impressive capacity maintenance, cycles studies were limited to 50 cycles. We thought employing this Li-ion pouch cell in prototype devices would fulfill the ultimate goal of applications: Thus fabricated Li-ion pouch cell (Fig. 9a) was used to activate an electronic toy-car for a load of 1.1 Wh on a smooth flooring tiles (Fig. 9b). To highlight the versatile application scope of the fabricated Li-ion pouch cell, we have demonstrated through energizing 40 LEDs (load = 0.12 Wh, ~15 h/charge) which may be useful for lighting applications and also running an electronic toy-car in coarse bitumen road at CSIR-CECRI, INDIA (Video demonstration in supplementary S1). During this demonstration it has been found that while illuminating the 40 LEDs, running of the toy-car consumed currents at the rate of 35 mA and 315 mA respectively from the thus fabricated pouch cell.

Supplementary video related to this article can be found at http://dx.doi.org/10.1016/j.jpowsour.2013.06.126.

4. Conclusions

Well dispersed LNMC cathode particles (size ~200 nm) with clear faceted, edge-blunted polyhedral morphology have been synthesized through a facile route employing toxic free mixed hydroxy-carbonate precursor. Thus obtained particles exhibited lower degree of cation mixing coupled with high degree of hexagonal ordering revealed from the clearly separated (006)/(102), (108)/(110) X-ray diffraction peaks. Lithium ion cell made using this cathode materials yielded high capacity of 187 mAh g^{-1} which can be categorically attributed to sharp edges of these particles explainable under the phenomenon of *shape-drive* through which charge flow, concentration activities may acquire dominance in the vicinity of sharp edges of the electrode through a process mimicking celebrated corona discharge. This hypothesis further gets corroborated from the report(s) of spherical particles of the same cathode system invariably yielding lower capacity. Motivated by the impressive cathode performance we fabricated pouch cell with this material for eventual applications in devices under moderate load conditions (0.12 Wh, 1.1 Wh) as demonstrated.

Acknowledgment

The author, P. Manikandan, acknowledges the Council of Scientific and Industrial Research (CSIR), New Delhi for granting the financial support for the above work in the form of a senior research fellowship and also our thanks to the Director, CSIR-CECRI, for the support.

References

[1] T.K. Nagaura, Prog. Batteries Sol. Cells 9 (1990) 209.
[2] J.M. Tarascon, D. Guyomard, G.L. Baker, J. Power Sources 44 (1993) 689–700.
[3] J. Breger, N. Dupré, P.J. Chupas, P.L. Lee, T. Proffen, J.B. Parise, C.P. Grey, J. Am. Chem. Soc. 127 (2005) 7529–7537.
[4] T. Ohzuku, Y. Makimura, Chem. Lett. 30 (2001) 642–643.
[5] S.H. Park, C.S. Yoon, S.G. Kang, H.S. Kim, S.I. Moon, Y.K. Sun, Electrochim. Acta 49 (2004) 557–563.
[6] Z. Wang, Y. Sun, L. Chen, X. Huang, J. Electrochem. Soc. 151 (2004) A914–A921.
[7] C.H. Chen, C.J. Wang, B.J. Hwang, J. Power Sources 146 (2005) 626–629.
[8] S.K. Martha, H. Sclar, Z.S. Framowitz, D. Kovacheva, N. Saliyski, Y. Gofer, P. Sharon, E. Golik, B. Markovsky, D. Aurbach, J. Power Sources 189 (2009) 248–255.
[9] M.V. Reddy, G.V. Subba Rao, B.V.R. Chowdari, J. Power Sources 159 (2006) 263–267.
[10] C.H. Lu, Y.K. Lin, J. Power Sources 189 (2009) 40–44.
[11] H. Ren, Y. Wang, D. Li, L. Ren, Z. Peng, Y. Zhou, J. Power Sources 178 (2008) 439–444.
[12] E.L. Uzunova, I.G. Mitov, G. Klissurski, J. Mater. Chem. 6 (1996) 1035–1040.
[13] F. Wu, M. Wang, Y. Su, L. Bao, S. Chen, J. Power Sources 195 (2010) 2362–2367.
[14] Y. Fujii, H. Miura, N. Suzuki, T. Shoji, N. Nakayama, J. Power Sources 171 (2007) 894–903.
[15] K. Yin, W. Fang, B. Zhong, X. Guo, Y. Tang, X. Nie, Electrochim. Acta 85 (2012) 99–103.
[16] F. Fu, G.L. Xu, Q. Wang, Y.P. Deng, X. Li, J.T. Li, L. Huang, S.G. Sun, J. Mater. Chem. A 1 (2013) 3860–3864.
[17] M. Uno, K. Ogawa, Y. Takeda, Y. Sone, K. Tanaka, M. Mita, H. Saito, J. Power Sources 196 (2011) 8755–8763.
[18] C. Delmas, I. Saadoune, A. Rougier, J. Power Sources 44 (1993) 595–602.
[19] Y.S. He, Z.F. Ma, X.Z. Liao, Y. Jiang, J. Power Sources 163 (2007) 1053–1058.
[20] J.N. Reimers, E. Rossen, C.D. Jones, J.R. Dahn, Solid State Ionics 61 (1993) 335–344.
[21] X. Wu, X. Li, Z. Wang, H. Guo, P. Yue, Y. Zhang, Appl. Surf. Sci. 268 (2013) 349–354.
[22] K. Nakamoto, Infrared and Raman Spectra of Inorganic and Coordination Compounds Part A: Theory and Applications in Inorganic Chemistry, fifth ed., John Wiley & Sons, 1997.
[23] N.V. Kosova, E.T. Devyatkina, V.V. Kaichev, J. Power Sources 174 (2007) 965–969.
[24] L.A. Riley, S.V. Atta, A.S. Cavanagh, Y. Yan, S.M. George, P. Liu, A.C. Dillon, S.H. Lee, J. Power Sources 196 (2011) 3317–3324.
[25] E. Zhecheva, R. Stoyanova, R. Alcăıntara, P. Lavela, J.L. Tirado, Pure Appl. Chem. 74 (2000) 1885–1894.
[26] R. Stoyanova, E. Zhecheva, S. Vassilev, J. Solid State Chem. 179 (2006) 378–388.
[27] K. Ben Kamel, N. Amdouni, A. Abdel-Ghany, K. Zaghib, A. Mauger, F. Gendron, C.M. Julien, Ionics 14 (2008) 89–97.
[28] P.J. Alonso, R. Alcala, J.M. Spaeth, Phys. Rev. B 41 (1990) 10902–10905.
[29] E. Shinova, R. Stoyanova, E. Zhecheva, G.F. Ortiz, P. Lavela, J.L. Tirado, Solid State Ionics 179 (2008) 2198–2208.
[30] M. Labrini, I. Saadoune, A. Almaggoussi, J. Elhaskouri, P. Amoros, Mater. Res. Bull. 47 (2012) 1004–1009.
[31] A.M.A. Hashem, A.E. Abdel-Ghany, A.E. Eid, J. Trottier, K. Zaghib, A. Mauger, C.M. Julien, J. Power Sources 196 (2011) 8632–8637.
[32] X. Han, Q. Meng, T. Sun, J. Sun, J. Power Sources 195 (2010) 3047–3052.
[33] H.F. Xiang, H. Wang, C.H. Chen, X.W. Ge, S. Guo, J.H. Sun, W.Q. Hu, J. Power Sources 191 (2009) 575–581.
[34] S.F. Lux, I.T. Lucas, E. Pollak, S. Passerini, M. Winter, R. Kostecki, Electrochem. Commun. 14 (2012) 47–50.
[35] J.H. Kim, C.S. Yoon, Y.K. Sun, J. Electrochem. Soc. 150 (2003) A538–A542.
[36] K. Cummings, P. Laws, E. Redish, P. Cookey, Understanding Physics, John Wiley & Sons, 2006.
[37] R.A. Serway, J.W. Jewett, Principles of Physics, fifth ed., Physical Science Mary Finch, 2006.
[38] K. Amine, I. Belharouak, Z. Chen, T. tran, H. Yummoto, N. ota, V. Myung, Y.K. Sun, Adv. Mater. 22 (2010) 3052–3057.
[39] S.S. Zhang, J. Power Sources 161 (2006) 1385–1391.
[40] H.H. Lee, Y.Y. Wang, C.C. Wan, M.H. Yang, H.C. Wu, D.T. Shieh, J. Power Sources 134 (2004) 118–123.